int21, rue d'Artois, F-75008 PARIS
http : //www.cigre.org

CIGRE US National Committee
2023 Grid of the Future Symposium

# Case Studies of the Stability Benefit of Grid Forming Inverters on Energy Storage Facilities

**N. EKNELIGODA, R. O'KEEFE**
**American Electric Power**
**USA**

**D. RAMASUBRAMANIAN**
**Electric Power Research Institute (EPRI)**
**USA**

**SUMMARY**

With the rapid growth of renewable generation, the application of power electronic converters is rising. However, this now massive penetration of inverter-based generation resources (IBR) has resulted in additional stability and operational challenges to the power grid unseen before. Power electronics inverters may be classified as either grid forming (GFM) or grid following (GFL). GFM inverters provide several advantages over GFL, as discussed in the literature, and are generally more suitable in weaker power grids. Understanding the application of GFM inverters and their stability properties in large-scale systems is of key importance. This paper investigates the stabilizing properties of GFM equipped battery installations on adjacent GFL wind and solar generation plants amid selected "weak-grid" network topologies by means of large-scale system simulations. GFM control is simulated using a positive sequence GFM model developed by the Electric Power Research Institute (EPRI). Various test cases are simulated to observe the stabilizing response of GFM inverters.

**KEYWORDS**

Grid-Forming, Inverter-Based Resource, System Stability, Generic Model, Positive Sequence, Weak-Grid

## I. Introduction

Electric power systems are experiencing rapid transition toward renewable power electronic-based generation systems. Conventional thermal generating units with synchronous machine interfaces

ncekneligoda@aep.com

to electric grids are being replaced by generation resources with power electronic interfaces generally termed *inverter-based resources* (IBR). As the penetration of IBRs, including wind, solar, and battery escalates, major operational challenges are posed to power grid operators. IBRs can respond quickly to changing conditions but generally provide little or no inertia to the systems. Because of low inertia, unexpected loss of generation events may result in immediate and severe frequency drops or even grid collapse. Thus, fast control of both active and reactive power plays an important and increasing role in stabilizing renewable-based power systems.

The electric power industry has been contemplating the introduction of grid-forming inverter technology as one means of addressing issues raised in consequence. The technology is enjoying increasing interest in North America and the rest of the world [1-3, 5-7]. In general, IBR control can be viewed either as grid-forming (GFM) or grid-following (GFL) [3, 5-6]. GFL, which to date has been universal in North American interconnections, is more suitable for grids with rigidly defined voltage magnitude and phase angle. GFL IBRs operate with phase lock loop (PLL) and fast current control loops but inverter current is determined based on the measurement of terminal voltage. Therefore, there is delay of feedback signals to the current control through the PLL and associated voltage calculation such that GFL control cannot adjust active and reactive current instantaneously in response to grid events. Hence, GFL-based IBR stable performance is dependent on grid stability, that is, avoidance of abrupt changes in voltage magnitude and phase.

In contrast to GFL, GFM inverters are more suitable in power grids where voltage magnitude and phase are not as rigidly maintained. GFM inverters' response to the power grid is near instantaneous in the transient time frame [3]. Depending on how specified and designed, GFM technology has the capability to either replicate or substitute for some of the rotating synchronous generation characteristics that have permitted secure and stable power systems until now [5-6]. The ability to establish a rigid voltage source in both magnitude and angle within the current capabilities of the inverter semiconductor is the essential aspect of GFM. This is in contrast to GFLs, which are contingent on a reasonably rigid voltage source to function in a stable fashion, and which rigid source they cannot themselves provide [6-7].

This paper investigates the stability benefit achieved through GFM inverters applied to energy storage resources in three different case studies. The example cases discussed here showing GFM capability were simulated using a generic positive sequence GFM stability model developed by Electric Power Research Institute (EPRI) [8-10]. The development of this model is based on the research work conducted jointly by EPRI and the Universal Interoperability for Grid-Forming Inverters (UNIFI) Consortium [8-9]. Positive sequence-based simulation is as important as electromagnetic transient (EMT) simulation, since it allows for large-scale system simulations to be conducted with greater computational efficiency. In [8-9], the EPRI GFM model results are compared with corresponding EMT simulations of a small-scale system. GFM capable battery inverter technology is available today [4] and there is much industry-wide discussion about the potential benefits of such GFM applications for system stability improvement [12]. GFM

experience is being gained in some small power system applications already [4, 12], and a version of GFM specifications has been published by the UNIFI Consortium [13-14].

The paper first summarizes the EPRI GFM generic model, discussing and illustrating the droop control mode. Droop control is the primary GFM control mode applied to generate results in the test cases of this paper. Three case studies showcasing GFM stabilizing capability are then presented that involve local areas of stability constrained IBRs within the context of large interconnected systems.

## II. Generic GFM Model

A generic positive-sequence GFM stability model has been devised by EPRI according to the most popular forms of GFM inverters used for coupling inverter-based resources to the power grid. This generic positive sequence GFM model can be configured according to three different types of control methodologies which have been discussed in the literature. These methods are:

1) Droop control
2) Virtual Synchronous Machine (VSM) control
3) Dispatchable Virtual Oscillator (dVOC) control

An underlying structural similarity across these three grid-forming methods [1-2] permits all three dynamic control modes to be integrated into the same generic model. An input control flag enables the user to select the type of GFM mode. In this paper, the droop control mode is applied. The block diagram of the droop GFM mode is shown in Figure 1. In Figure 1, blue color variables indicate input variables from the network to the control structure. The orange color represents the output variables from the control to the network structure. Similarly, the green color shows the variables that can pass between different components in the structure and the purple color represents input reference values. The color red is used for state variables. All other variables are either local variables or control gains/flag settings. The xy reference frame is the real – imaginary coordinate frame of the network (also known as αβ frame) while the dq reference frame is the coordinate frame of the control. The relative angle between these reference frames is denoted by the control variable $\theta inv$.

EPRI has verified all three control mode results with EMT simulation in a small test system [8-9]. The goal of this paper is to apply the GFM model to real-life large-scale power system studies wherein different GFL wind and solar plants exhibit unstable performance during certain planning event contingencies unless the generation is curtailed to lower levels. The specific GFM model parameter values applied here are listed in the Appendix. It should be understood, that at present, the positive sequence generic GFM model described here does not necessarily represent any actual equipment being offered by equipment vendors, nor should it be construed that such offerings are available at present from any vendor.

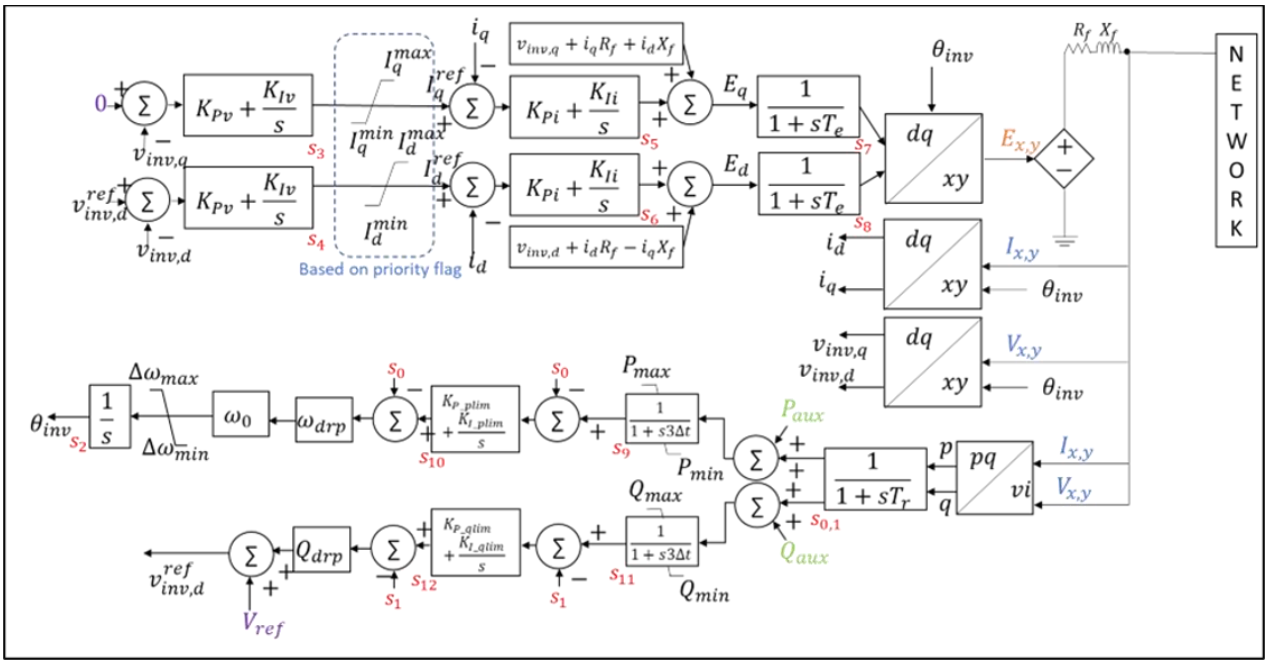


Figure 1. Generic model of droop-based GFM

## III. Case Study #1 Description and Results

Three type 3 wind farms are interconnected at a common 230 kV station (POI) with two exit paths, as shown in Figure 2. A N-1-1 contingency (marked by dashed lines) puts all three wind farms radially into a 230/138 kV transformer one station away, causing low voltage and instability. The generation capacity of the wind farms is 330 MW. This system is unstable after the N-1-1 contingency when total wind plant loading is above 250 MW.

In Figure 2, the line from bus 3 to bus 4 is initially out of service while the bus 1 to bus 2 line is faulted and cleared leaving the wind farms connected to the larger power system only through the 138 kV path at bus 5.

### a) Operation of wind farms without GFM

Initially, the simulation is run without a GFM battery attached to bus 1. In this first case, the wind total generation level is set at 265 MW. Voltage and power versus time plots are shown in Figure 3 indicating partial voltage collapse before sufficient reactive power can be mustered by the wind farms to bring voltage back to the normal range.

### b) Operation of wind farms with GFM

To stabilize the case at this and higher generation levels, a battery IBR with a 100 MVA GFM controlled inverter is added to the 230 kV bus 1 as shown in Figure 2. The GFM control is configured according to Figure 1 for closed-loop droop mode regulation of voltage. The same N-1-1 case is run again at a higher wind generation level increased from 265 MW to 290 MW. At

simulation time *t=0*, the GFM active/reactive injection is set to zero. Figures 4 and 5 show the voltage and active/reactive power variation of the wind farms and the GFM. The GFM contribution stabilizes the case, supplying sufficient reactive in support of the three wind farms to prevent the collapse.

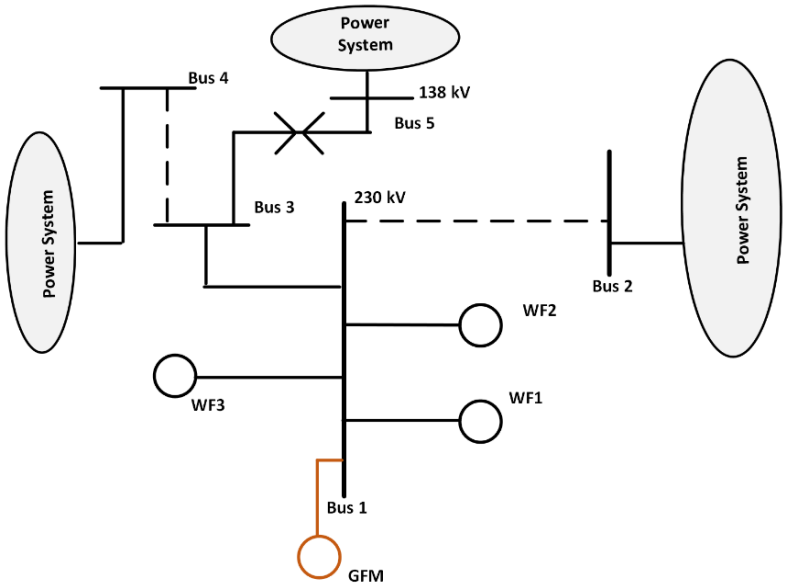


Figure 2. Case Study #1 system configuration

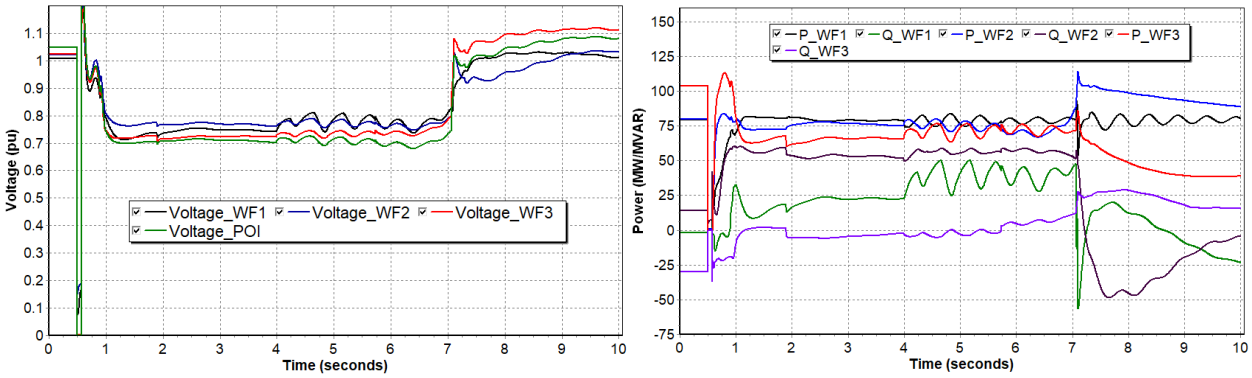


Figure 3. Voltage (left) and power (right) of WF 1, WF 2, and WF 3 at 80 MW, 80 MW, and 105 MW generation without GFM

In Figures 6 and 7, the simulation is repeated with total wind generation set to 100 percent of wind farm capacities (330 MW). The GFM is again set to zero active/reactive power initially. Here, the GFM again stabilizes the case though it is necessary to increase the GFM transformer rating from 100 MVA to 500 MVA to enable the GFM to supply the additional reactive power needed to stabilize the case at the 330 MW level. This example also highlights the necessity of increased

transient reactive power deliverability in the region that is required to maintain wind farm active power after the fault clears.

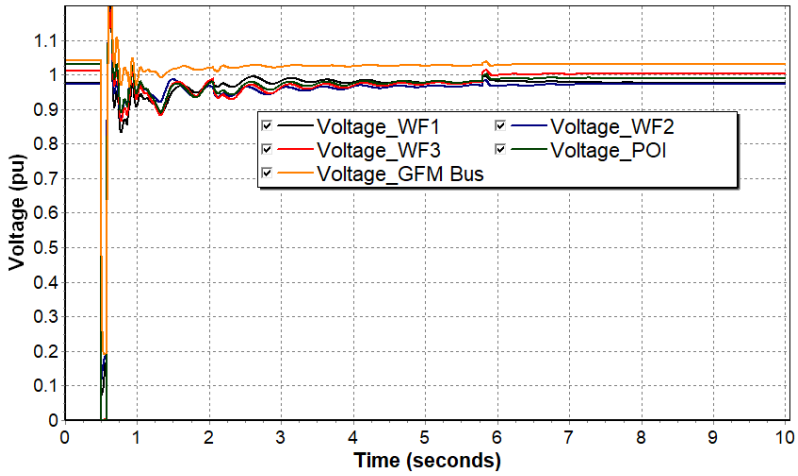


Figure 4. Voltage of WF 1, WF 2, and WF 3 at 85 MW, 85 MW and 120 MW wind generation with GFM

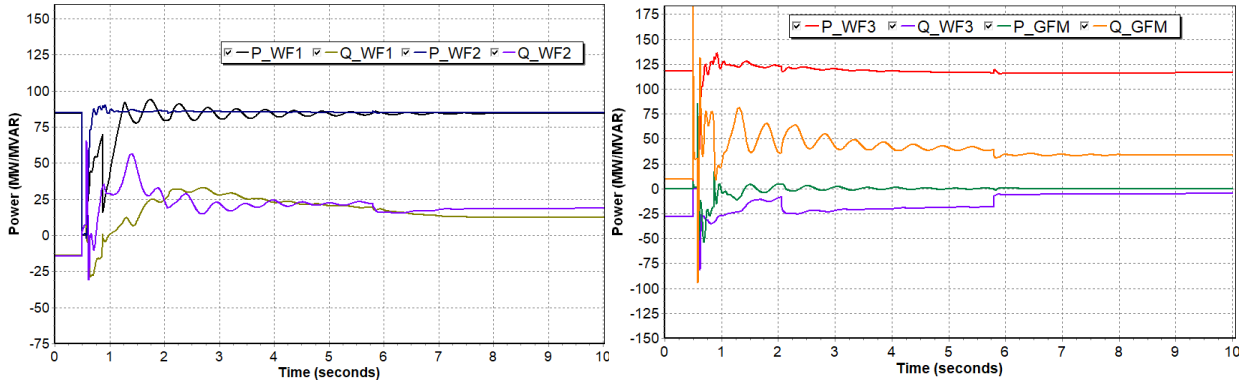


Figure 5. WF 1 and WF 2 power (left) and WF 3 and GFM (right) at 85 MW, 85 MW, and 120 MW wind generation with GFM

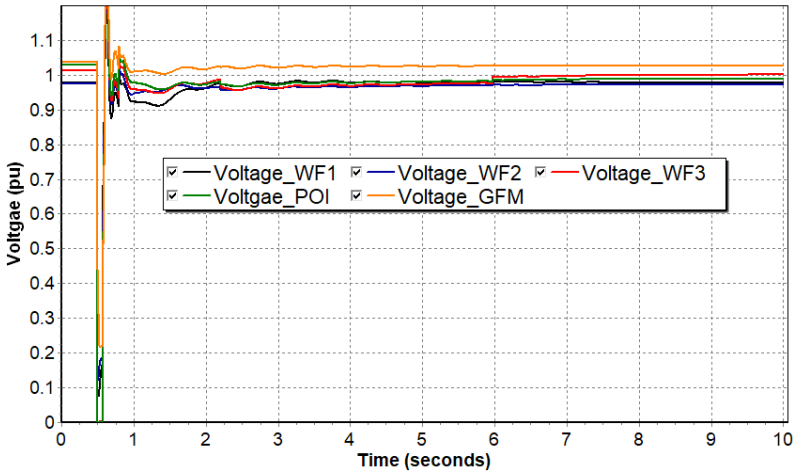


Figure 6. Voltage of WF 1, WF 2, and WF 3 at 99 MW, 99 MW and 132 MW wind generation with GFM

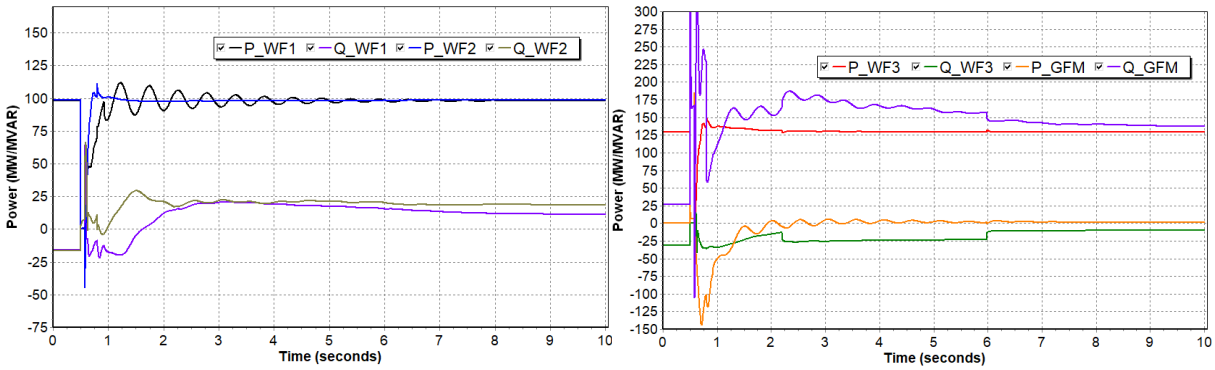


Figure 7. WF 1 and WF 2 power (left) and WF 3 and GFM (right) at 99 MW, 99 MW and 132 MW wind generation with GFM

### c) Testing the case with synchronous condenser

As a point of comparison, the GFM is replaced with a synchronous condenser having dynamic modeling data of the machine and high-speed static excitation system from a recent synchronous condenser project. However, the synchronous condenser is unable to stabilize the system at the initial 265 MW wind generation level of Figure 3 and, in fact, becomes unstable itself as shown in Figure 8.

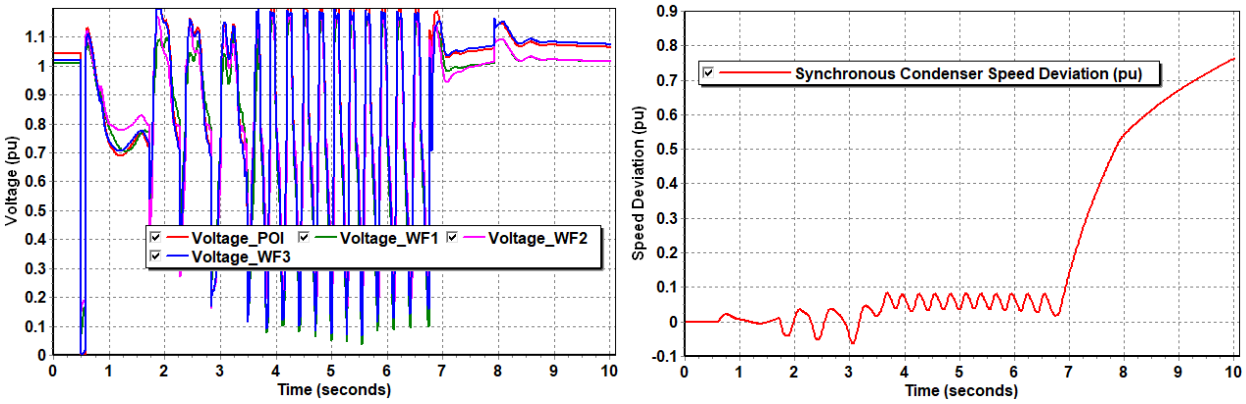


Figure 8. Voltage (left) of WF1, WF2, and WF3, and synchronous condenser speed (right) at 80 MW, 80 MW and 105 MW wind generation with synchronous condenser replacing GFM

## IV. Case Study #2 Description and Results

This is a case of some older WFs consisting of both Type 1 and Type 3 at a 138 kV station (bus 1) that has two 138 kV lines exiting and two autotransformers stepping up to 345 kV as shown in Figure 9. The contingency is N-1-1 involving the two autotransformers, one of which is a prior outage and a three-phase normally cleared fault on 138 kV windings of second transformer

removes it. Remaining connections to the interconnected power system are two the 138 kV lines at buses 3 and 4.

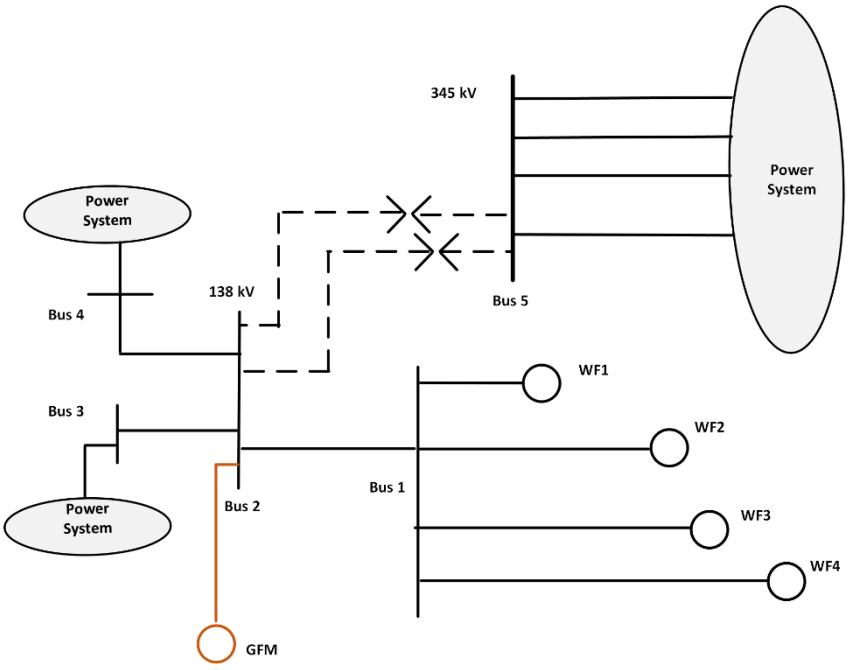


Figure 9. Case Study #2 system configuration

The wind farms totaling 523 MW are dispatched to 100 percent of their MW capacity and an oscillatory response ensues (Figure 10). A 100 MVA GFM battery located at the same 138 kV POI as the wind farms is able to more quickly damp out the poorly damped oscillatory response of the wind farms (Figure 11).

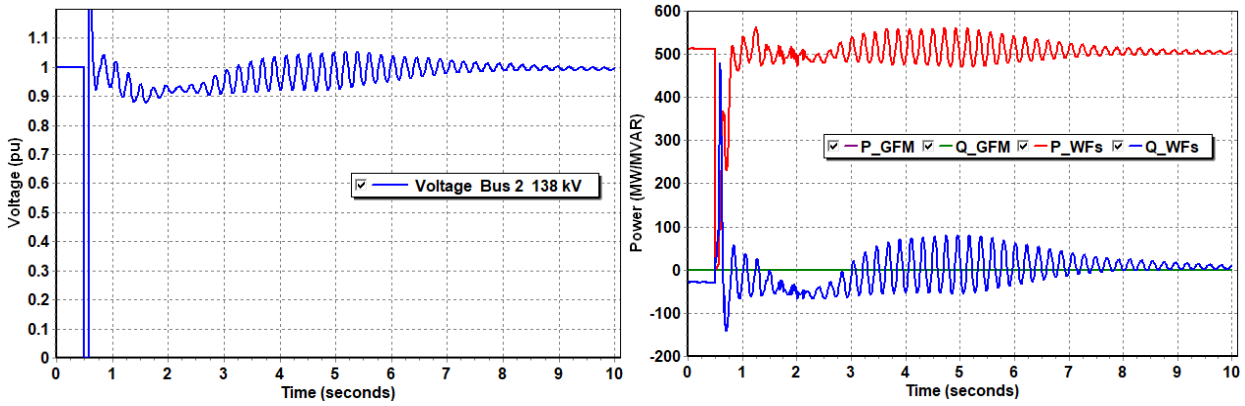


Figure 10. POI voltage (left) and sum of wind generation MW/MVAR (right) without GFM battery

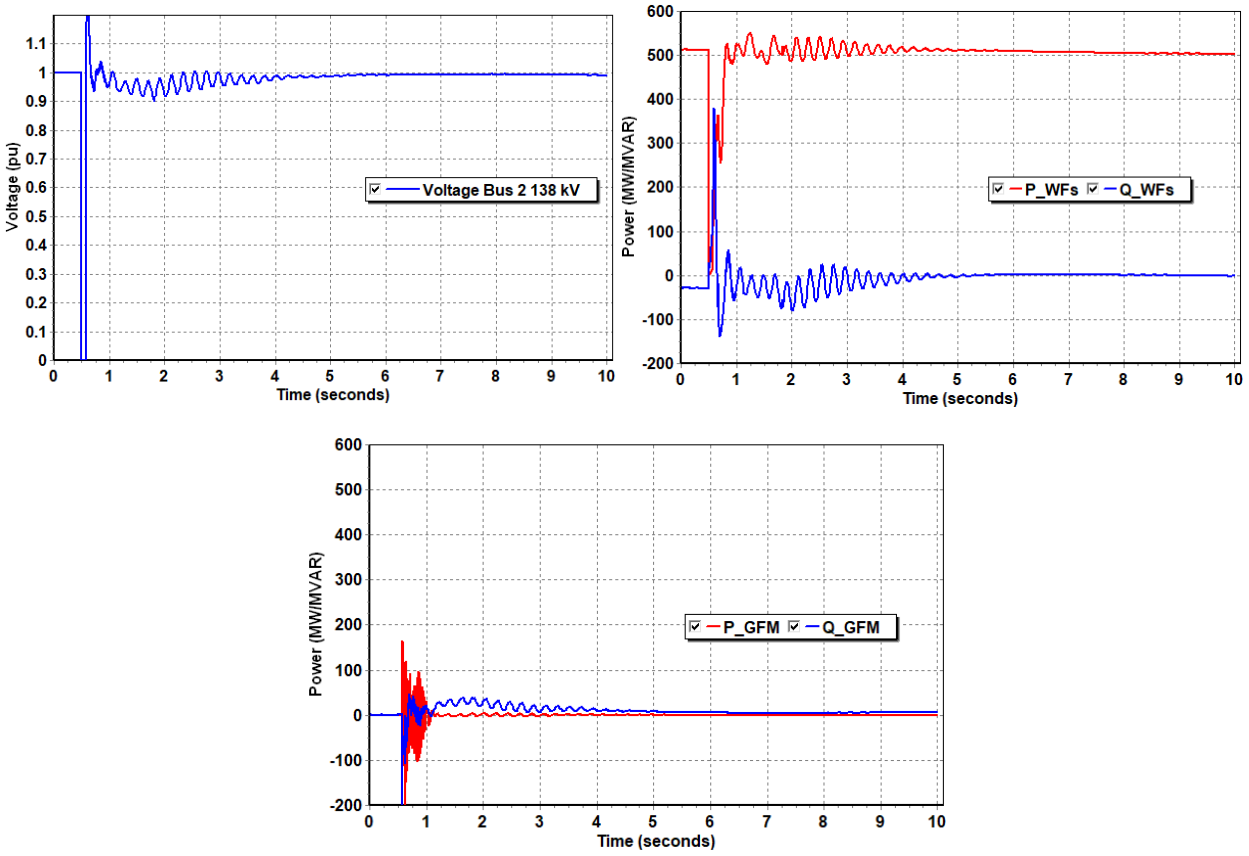


Figure 11. POI voltage (left), sum of wind generation MW/MVAR (right), and GFM MW/MVAR (bottom) with GFM battery

## V. Case Study #3 Description and Results

This is a slightly more complicated configuration involving three wind farms and a solar farm totaling 515 MW strung out along a 138 kV corridor as shown in Figure 12. A single GFM battery is located at the same POI as the solar farm which is the most centrally positioned IBR. The contingency is again N-1-1 involving two of three 138 kV lines exiting the area of these IBRs. One 138 kV line at bus 4 is a prior outage while a three-phase normally cleared fault removes the second 138 kV line between buses 1 and 7. The remaining 138 kV line from bus 5 to the interconnected power system is the weakest path exiting the area.

Here, instability of the wind farms and solar farm is seen as an alternating rapid voltage decline and recovery as the IBRs shift between normal and ride-through modes (Figure 13). A 100 MVA GFM battery located at the same POI as the solar farm is able to supply sufficient stiffness to the 138 kV voltage to allow the IBRs to operate in a stable fashion (Figure 14).

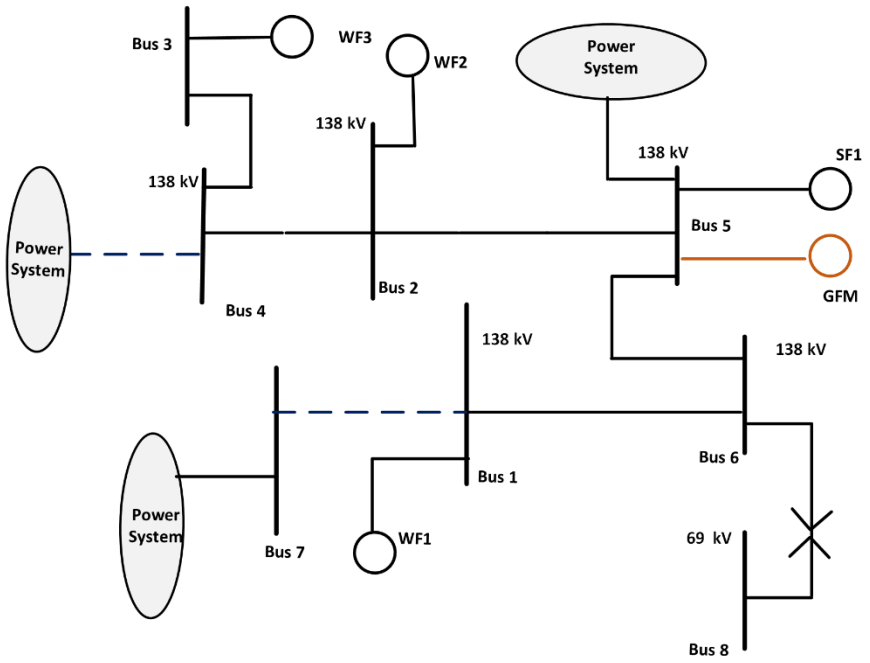


Figure 12. Case Study #3 system configuration

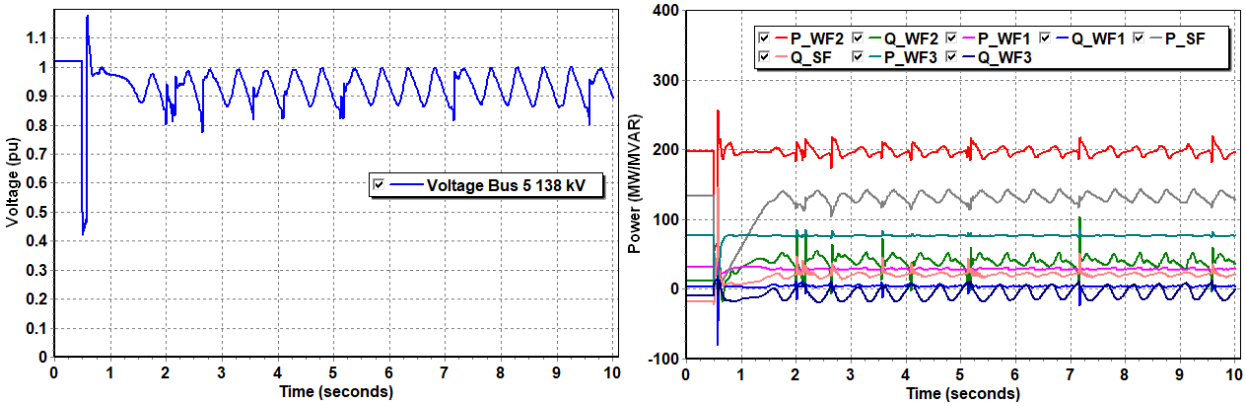


Figure 13. Solar farm POI voltage (left) and wind/solar generation MW/MVAR (right) without GFM battery

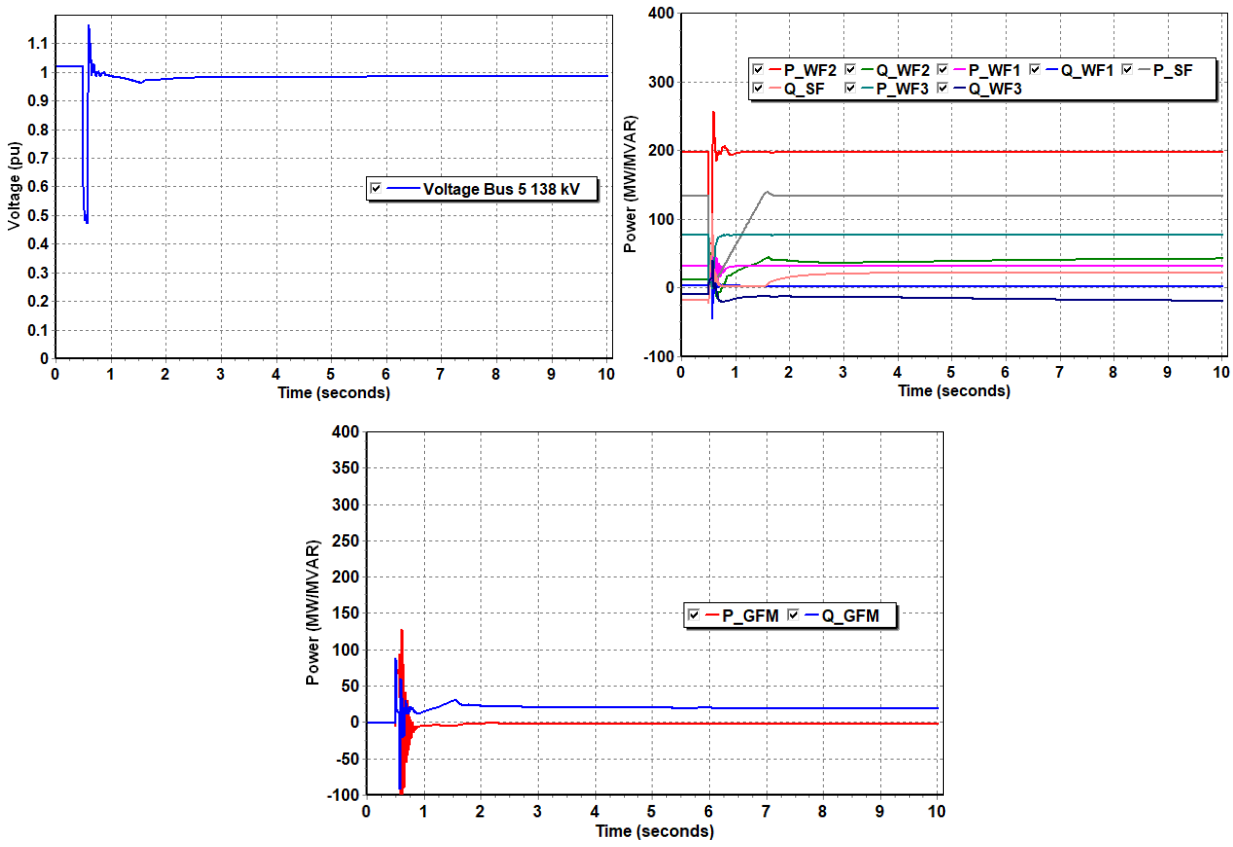


Figure 14. POI voltage (left), wind/solar generation MW/MVAR (right), and GFM MW/MVAR (bottom) with GFM battery with GFM

## V. Conclusion

A battery inverter equipped with GFM droop control is seen as able to effectively stabilize GFL wind and solar IBRs under various post-contingency "weak" grid conditions. The case studies each exhibit a different form of instability varying between partial voltage collapse, poorly damped oscillations, and rapid unstable mode shifting. The GFM is able to begin with zero active and reactive power injection and drive the system to a stable operating point by short-term dynamic active and reactive injection either without continuing power injection or, with one exception, minimal continuing reactive contribution.

The results discussed here are limited to the droop-based control mode integrated into the GFM model. Application of other control modes (dVOC and VSM) to the above discussed unstable cases, and study of GFM behavior in other unstable events are directions of possible continuing work. Determination of optimal GFM sizing as well as the appropriate number and placement of GFMs to aid larger unstable groupings of GFL IBRs are some other possible future directions.

GFM device control tuning is also important and one shouldn't expect a particular GFM inverter control tuning to always function effectively in all scenarios to rescue a system from instability. As with other IBR devices, GFM devices also need to be tuned appropriately for the location,

conditions, and events being evaluated. Finally, a GFM device may not be the only solution to challenges identified in this paper and alternative solution options can also be considered.

## ACKNOWLEDGMENTS

The development of the generic GFM model and its performance validation was supported, in part, by the U.S. Department of Energy's Office of Energy Efficiency and Renewable Energy (EERE) under the Solar Energy Technologies Office Award Number 38637, in part by the U.S. Department of Energy's Solar Energy Technologies Office Award Number DE-EE0009025 and, in part, by EPRI's Research Program 173: Bulk System Integration of Renewables and Distributed Energy Resources.

## BIBLIOGRAPHY

[1] Guilherme Santos Pereira, Fabien Benavent, Jakub Witkowski and Gregoire Prime, "Taking advantage of grid-forming BESS behavior during major outages: contribution to improve the share of renewable energy in French isolated power systems," 2022, CIGRE Science & Engineering Journal.

[2] S. Sproul, M. Modi, S. Cherevatskiy, A. Jalali, S. ZaBihi, J. Zimmermanni, A. Tuckey, "System strength support using grid-forming energy storage to enable high penetrations of inverter-based resources to operate on weak networks," 2022, CIGRE Science & Engineering Journal.

[3] North American Electric Reliability Corporation, "White Paper: Grid Forming Technology Bulk Power System Reliability Considerations," NERC, Atlanta, GA, 2021.

[4] North American Electric Reliability Corporation, "Reliability Guideline: Performance, Modeling, and Simulations of BPS-Connected Battery Energy Storage Systems and Hybrid Power Plants," NERC, Atlanta, GA, 2021.

[5] R. H. Lasseter, Z. Chen, "Grid-Forming Inverters: A Critical Asset for the Power Grid," *IEEE Journal of Emerging and Selected Topics in Power Electronics*, vol. 8, no. 2, pp. 925–935, June 2020.

[6] Y. Li, Y. Gu and T. C. Green, "Revisiting Grid-Forming and Grid-Following Inverters: A Duality Theory," IEEE Transaction on Power Systems, vol. 37, no. 6, pp. 4541–4554, Nov.2022.

[7] C. Cardozo, Y. Vernay, G. Denis, T. Prevost, M. Zubiaga, J. J. Valera, "OSMOSE: Grid-Forming performance assessment within multiservice storage system connected to the transmission grid," 2020, CIGRE Science & Engineering Journal.

[8] D. Ramasubramanian and Q. Zhang, "Generic Grid Forming (GFM) Positive Sequence Models for Inverter Based Resources," EPRI Memorandum, Palo Alto, CA, 2022.

[9] D. Ramasubramanian, "Memo on Proposal for Generic GFM Model," December 2021. [Online]. Available: https://www.wecc.org/_layouts/15/WopiFrame.aspx?sourcedoc=/Administrative/Memo%20on%20Proposal%20for%20Generic%20GFM%20Model_v2.pdf&action=default&DefaultItemOpen=1.

[10] Electric Power Research Institute, "EMT and Positive Sequence Domain Model of Grid Forming PV Plant (GFM-PV)," EPRI, Palo Alto, CA, 2021, 3002021787.

[11] D. Ramasubramanian, "Modeling of grid forming (GFM) IBR and frequency response in a 100% IBR Grid," October 2021. [Online]. Available:

https://www.wecc.org/_layouts/15/WopiFrame.aspx?sourcedoc=/Administrative/WECC%20Grid%20Forming%20Inverter%20Based%20Resources%20.1.pdf&action=default&DefaultItemOpen=1.

[12] J. Matevosyan, "Survey of Grid-forming Inverter Applications," G-PST/ESIG Webinar Series

[13] B. Kroposki, "Understanding Grid-forming Inverter Specifications," February 2023. [Online]. Available: file:///C:/Users/s341378/Desktop/2021MDWG_TPL001/Other%20Material/Understanding-Grid-forming-Inverter-Specifications-Ben-Kroposki.pdf

[14] National Renewable Energy Laboratory (NREL) News, "NREL To Lead Grid-Forming Inverter Consortium, Streamlining Renewable Integration at All Scales," [Online]. Available: https://www.nrel.gov/news/program/2021/nrel-to-lead-grid-forming-inverter-consortium.html

## APPENDIX

*Table 1. Generic GFM Model Parameters*

| **Parameter** | **Description** | **Units** | **Default Value** |
|---|---|---|---|
| MVA rating | IBR rating | MVA | 100.0 |
| $R_f$ | Filter resistance | pu on MVA rating | 0.002 |
| $X_f$ | Filter reactance | pu on MVA rating | 0.2 |
| $V_{dip}$ | State freeze threshold | pu | 0.85 |
| $T_{frz}$ | Time to keep state frozen | s | 0.5 |
| $I_{max}$ | Maximum current magnitude | pu | 1.2 |
| PQflag | Current priority | - | PSLF model = 0 – P priority, 1 – Q priority |
| $\omega_0$ | Nominal angular frequency | rad/s | 376.99 |
| $\Delta\omega_{max}$ | Maximum value of frequency deviation | rad/s | 75.0 |
| $\Delta\omega_{min}$ | Minimum value of frequency deviation | rad/s | -75.0 |
| $\omega_{drp}$ | Frequency droop percent | - | 0.033 |
| $Q_{drp}$ | Voltage droop percent | - | 0.045 |
| $T_r$ | Transducer time constant | s | 0.005 |
| $T_e$ | Output state time constant | s | 0.005 |
| $K_{Pi}$ | Current control proportional gain | - | 0.5 |
| $K_{Ii}$ | Current control integral gain | - | 20.0 |
| $K_{Pv}$ | Voltage control proportional gain | - | 3.0 |
| $K_{Iv}$ | Voltage control integral gain | - | 10.0 |
| $P_{max}$ | Maximum active power | pu on MVA rating | 1.0 |
| $P_{min}$ | Minimum active power | pu on MVA rating | -1.0 |
| $K_{P\_plim}$ | Proportional gain for P limits | - | 5.0 |
| $K_{I\_plim}$ | Integral gain for P limits | - | 30.0 |
| $Q_{max}$ | Maximum reactive power | pu on MVA rating | 1.0 |
| $Q_{min}$ | Minimum reactive power | pu on MVA rating | -1.0 |
| $K_{P\_qlim}$ | Proportional gain for Q limits | - | 0.1 |
| $K_{I\_qlim}$ | Integral gain for Q limits | - | 1.5 |
| Control (PSLF) ICON (M) (PSSE) | Control flag to choose GFM structure | - | 1 – Droop 2 – VSM 3 – dVOC |